Unresolved transition array based water window soft x-ray source by laser-produced high-*Z* plasma

Takeshi Higashiguchi[1], Padraig Dunne[2], and Gerry O'Sullivan[2]

[1]*Department of Advanced Interdisciplinary Sciences, Center for Optical Research ¥& Education (CORE), and Optical Technology Innovation Center (OpTIC), Utsunomiya University, Yoto 7-1-2, Utsunomiya, Tochigi 321-8585 Japan*

[2]*School of Physics, University College Dublin, Belfield, Dublin 4, Ireland*

ABSTRACT

We demonstrate a table-top broadband emission water window source based on laser-produced high-Z plasmas. Resonance emission from multiply charged ions merges to produce intense unresolved transition arrays (UTAs) in the 2 to 4 nm region, extending below the carbon K edge (4.37 nm). Arrays resulting from $n = 4–n = 4$ transitions are overlaid with $n = 4–n = 5$ emission and shift to shorter wavelength with increasing atomic number. An outline of a microscope design for single-shot live cell imaging is proposed based on a bismuth plasma UTA source, coupled to multilayer mirror optics. At power densities available from "table-top" solid-state lasers, comparison of emission from a number of targets has shown that $3d–4f$ UTA in zirconium plasmas have highest overall brightness and in an imaging system based on reflective multilayer mirrors, may, depending on bandwidth, have superior performance than either line or broader-band sources.

Keywords

Unresolved transition array (UTA), water window, soft x-ray, laser-produced plasma, high-*Z*

1. Introduction

Development of shorter wavelength sources in the extreme ultraviolet (EUV) and soft x-ray spectral regions has been motivated by their application in a number of high profile areas of science and technology. One such topic is the challenge of three-dimensional imaging and single-shot flash photography of microscopic biological structures, such as cells and macromolecules, *in vivo* [1]. For x-ray microscopy, the x-ray source should emit a sufficient photon flux to expose the image of the biological sample on the detector. To date the most practical light source of high-power, high-brightness x-rays has been radiation from synchrotrons and more recently from free electron lasers (FEL) [2]. Table-top sources using ethanol sprays and liquid nitrogen droplets are being developed for use with zone plates for transmission microscopy. Recently λ = 2.48 nm narrowband emission from a liquid-nitrogen-jet laser-plasma [3] was successfully combined with state-of-the-art normal-incidence multilayer condenser optics and 20-nm zone-plate imaging optics to demonstrate laboratory water-window x-ray microscopy [4] with resolution less than 25 nm and synchrotron-like image quality on biological and soil science samples. In addition, the development of a high-brightness source based on a focused electron-beam impacting a liquid water jet resulting in λ = 2.36 nm emission has also been reported [5]. However, the total collected energy is low, when one combines the narrow line emission with the low reflectivity of the collector mirror. As a result long exposures are needed to record an image and there is not yet published evidence of single-shot

exposures using a laboratory-scale source. To overcome the low efficiency imposed by line sources, we propose using high power water-window emission from laser-produced high-Z plasmas, analogous to the scheme used for efficient, high-volume manufacturing EUV sources.

Efficient, high-power extreme-ultraviolet (EUV) sources for semiconductor lithography at 13.5 [6] and 6.7 nm [7-9] based on laser-produced plasmas have been demonstrated in high-volume manufacturing of integrated circuits (IC) having node sizes of 22 nm or less [10]. Plasmas of the high-Z elements Sn and Gd produce strong resonant emission due to $4d$–$4f$ and $4p$–$4d$ transitions at 13.5 nm and 6.7 nm, respectively, which overlap in adjacent ion stages to yield an intense unresolved transition array (UTA) in their spectra. The in-band high-energy emission is thus attributable to hundreds of thousands of near-degenerate resonance lines lying within a narrow wavelength range.

Before discussing the high-power water window source, it is important to summarize the characteristics of efficient UTA light sources used in the 5 to 15 nm region. All are based on $n = 4$–$n = 4$ ($4d$–$4f$ and $4p$–$4d$) transitions that overlap to generate an intense UTA. For efficient 13.5-nm operation, which corresponds to a photon energy $h\nu \approx 92$ eV, it is important to produce an optimum plasma electron temperature of 30–50 eV. The rare-earth elements of gadolinium (Gd, $Z = 64$) and terbium (Tb, $Z = 65$) produce strong emission near $\lambda = 6.7$ nm ($h\nu \approx 183$ eV) which is maximized at electron temperatures in the 100–120 eV range depending on initial focusing conditions [7-9]. The spectral behavior of Gd and Tb plasmas is expected to be largely similar to that of Sn plasmas, because in the temperature range of interest, both are dominated by $4d$ open-shell ions. Although the conversion efficiency (CE) from the input laser energy to the output in-band EUV emission energy depends on the bandwidth (BW) of the reflection coefficient of the multilayer mirror (MLM), the maximum CEs have been observed to be higher than 1%. Because it moves to shorter wavelength with increasing atomic number, Z, the $n = 4$–$n = 4$ UTA is expected to lie in the water window if higher Z elements from $Z = 79$ (Au) to $Z = 83$ (Bi) are used [11-13]. Higher Z elements such as uranium also emit in the water window but their radioactivity prohibits their use. Much of the previous work on high-Z plasmas has concentrated on the production of quasicontinuum spectra at moderate laser intensities, employing electron temperatures below 100 eV [14-16].

In this paper, we report the efficient water window source by strong UTA band emission in laser-produced high-Z plasmas. Our proposed procedure for producing the water window emission is expected to be efficient and scalable in output yield. We have initiated a number of experiments to explore how this emission may be optimized in practice.

2. Experimental setup

To evaluate the spectral behavior, two Nd:YAG lasers operating at 1064 nm produced maximum pulse energies of 200 mJ for a pulse duration of 150 ps (FWHM) and 400 mJ at a pulse duration of 10 ns (FWHM), respectively. The laser was focused perpendicularly onto a target with a 10-cm focal length lens. The maximum focused intensity was approximately 1×10^{14} W/cm^2 at a constant focal spot diameter of 30–40 μm (FWHM). Under these conditions the maximum electron temperature attainable is predicted within the collisional radiative (CR) plasma regime to be greater than 3 keV and the corresponding maximum ion stage close to fifty times ionized [17]. In practice however, the ion stages responsible for the observed emission will be lower as the bulk of the emission is produced during the recombining expanding phase and because of the finite time required to attain the maximum stage consistent with the CR model predictions. The laser was operated in single shot mode. A flat-field grazing incidence spectrometer with 2400 grooves/mm variable line space grating was positioned at 45° with respect to the incident laser axis. Time-integrated spectra were measured by a thermoelectrically cooled back-illuminated x-ray CCD camera. The typical spectral resolution was better than 0.005 nm [18,19].

3. Au, Pb, and Bi plasmas

Figures 1(a)–1(c) show time-integrated spectra from Au, Pb, and Bi plasmas at a laser intensity of 1 × 10^{14} W/cm^2 with a 150-ps pulse duration. Time-integrated EUV spectra between 1 and 6 nm from each element display strong broadband emission near 4 nm, which is mainly due to $n = 4–n = 4$ transitions from ions with an open $4f$ or $4d$ outermost subshell, together with broadband emission around 2–4 nm due to $n = 4–n = 5$ transitions from multi-charged state ions with an outermost $4f$ subshell. The latter merge to form a structured feature from which the contributing ion stages may be readily inferred. The intensity of the $n = 4–n = 4$ UTA emission is higher than that of the $n = 4–n = 5$$ emission. The atomic number spectral dependence is summarized in Fig. 1(d). The predicted photon energy of each experimental peak wavelength was shifted to higher photon energy with increasing atomic number. Neither the emission spectra nor the plasma electron temperatures, however, have been optimized, as shown below. The emission intensity of the $n = 4–n = 5$ transitions, however, was compared with that of the $n = 4–n = 4$ UTAs.

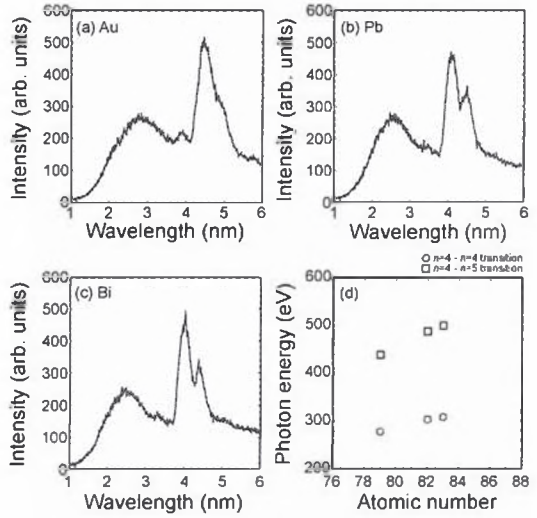

Fig. 1. Time-integrated spectra from the picosecond-laser-produced high-Z plasmas by use of Au (a), Pb (b), and Bi (c), and the atomic number dependence on the photon energies of peak emission of the $n = 4–4$ transition (circles) and the $n = 4–5$ transition (rectangles).

The strong emission at 3.15 nm due to the $n = 4–n = 4$ UTA in Bi plasmas may be coupled with a Sc/Cr MLM with a reflection coefficient of 15% [20]. The variation of this emission with electron temperature was calculated with Cowan's suite of atomic structure codes in order to predict its evolution with increasing laser flux [21]. The predicted spectral evolution as a function of electron temperature is summarized in Fig. 2. In this figure the spectra generated for each ion stage are based on excited state populations that allow for electron temperature assuming a Boltzmann distribution. These spectra are then weighted by an ion fraction appropriate to that temperature, calculated assuming CR equilibrium to yield the distributions shown.

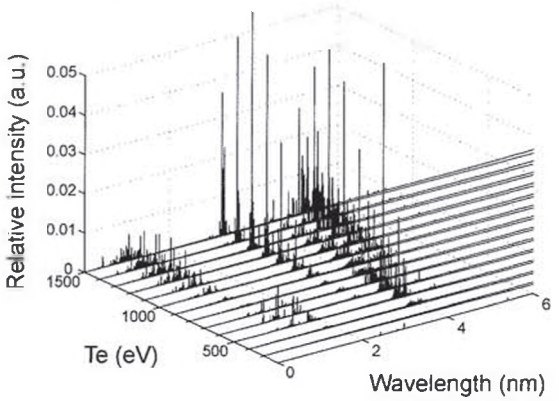

Fig. 2. Calculated spectral variation as a function of electron temperature.

To explain the Bi spectra, we compare the results of calculation for some experimental temperatures with the experimental spectrum, as shown in Fig. 3(a). Four regions corresponding to emission peaks are identified. Note that this spectrum is integrated both spatially and temporally over the duration of the laser pulse. The emission in region "1" results primarily from $4f–5g$ transitions in ions with an open $4f$ subshell, i.e., stages lower than Bi^{35+}. The emission in regions "2" and "3" comes from $4p–4d$ and $4d–4f$ transitions in ions with an open $4d$ subshell (Bi^{36+}–Bi^{45+}), and calculations show that the higher energy feature results from the more highly ionized species (> Bi^{42+}). The emission in region "4" is again associated mainly with $4d–4f$ emission from lower stages with an open $4f$ outmost subshell. Thus the

bulk of the emission, especially from regions "1" and "4", is associated with the recombining phase of the expanding plasma plume. In this figure we show for comparison spectra calculated for steady state electron temperatures of 180 and 700 eV, while the higher temperatures are required to generate the emission in region "2", the calculations verify that both the longer and shorter wavelength features are consistent with much lower plasma temperatures.

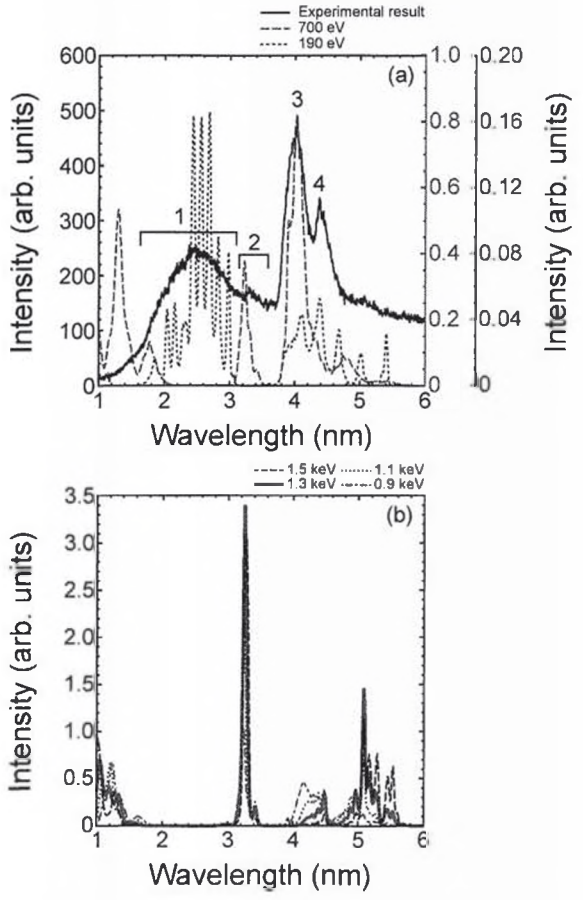

Fig. 3. Spectral behaviors of the Bi plasmas in the laser intensity dependence on the observed emission spectra (a), the peak wavelength of the $n = 4$–4 transition (circles) and the $n = 4$–5 transition (rectangles) (b).

In Fig. 3(b) calculated spectra at different electron temperatures higher than 900 eV are presented. Our calculations show that high-Z plasmas, at an electron temperature lower than 700 eV, as shown in Fig. 3(a), radiate strongly near 3.9 nm. However, in the case of higher electron temperatures, from 800 to 1500 eV, the strongest emission is expected at around 3.2 nm, suitable for coupling to Sc/Cr MLMs [20]. Thus for an optimized source, we should produce a plasma at a higher electron temperature plasma of around 1 keV. The intensity of the Bi plasma emission in our experiment was compared with 2.48-nm nitrogen line emission from a Si_3N_4 planar target, in the same experimental setup, and was observed to be 1.2 times higher within a bandwidth of 0.008 nm (FWHM) [20,22] even though the plasma electron temperature was much lower than the optimum value.

4. Proposal by Bi plasma source

Taking the experimental and numerical results into account, we now propose a high brightness, high power water window source for single shot imaging at the laboratory scale. Our proposed method has the advantage that the EUV energy efficiency and atomic number dependence can be scaled based on the fundamental properties of the plasma source. The electron temperature, T_e, in a high-Z plasma rises with increasing laser intensity as $T_e \propto (I_L\lambda_L^2)^{0.4}$, where I_L and λ_L are the laser intensity and wavelength, respectively [17]. To produce not only a Bi plasma with a high electron temperature of the order of 1 keV but also one that has low density and is optically thin, we should switch to a CO_2 laser operating at a wavelength of 10.6 μm due to the low critical density of 1×10^{19} cm^{-3} attainable [23], with a pulse duration to permit ionization to the appropriate ion stages (Bi^{36+}–Bi^{45+} i.e., > 150 ps), while at the same time maintaining a laser intensity of the order of 10^{13} W/cm^2 [24]. In addition, for this proof of principle, we propose a dot Bi target with a diameter less than 20 μm with a thickness less than 1 μm to generate a microplasma (to fulfill the requirements for high brightness and a point source) as the expected focal spot size will be the order of 100 μm in the case of the CO_2 laser wavelength of 10.6 μm. Because of the broadband nature of the emission, zone plate components cannot be used, so one possible solution would be to use a transmission planar x-ray nano-waveguide to image the sample [25]. To achieve high resolution in the recorded image, we should also switch the recording device from x-ray

CCD cameras to sensitive EUV resists to overcome the resolution limitation of the CCD pixel size, coupled with Schwarzschild optics, consisting of Sc/Cr MLMs with a reflection coefficient of the order of 15% around 3.2 nm [20]. Although our proposal is based on a simple microscope construction, the key component is the UTA emitted at 3.2 nm from a hot dense Bi plasma point source, combined with Sc/Cr MLMs and sensitive EUV resists based on photochemical reaction [26,27].

5. Zr plasmas

Two key aspects emerged from experimental studies on Bi. The first was that the high plasma temperatures required to produce the ion stages involved (Bi^{36+}–Bi^{45+}) necessitated the use of a very high laser flux higher than 10^{13} W/cm^2 at λ = 10.6 μm. Such fluxes are not currently available in ns pulses from "table-top" laser systems and the realization of a Bi plasma source is predicated on the future development of new high pulse energy CO_2 lasers with pulse durations of around one nanosecond [18]. The second was that spectra obtained at lower laser power densities with plasmas produced by a 10-ns duration Nd:YAG laser pulse contained a large contribution from Δn = 1, 4*f*–5*g* transitions from significantly lower ion stages in the 2–3.5 nm region that was actually comparable in intensity to the UTA emission from Δn = 0, n = 4–n = 4 transitions centered near 4.0 nm. This observation suggested the feasibility of using the emission of Δn = 1 transitions in other elements as possible candidates for water window sources. Indeed, such transitions in laser produced plasmas formed on Ar and Kr gas jets are in widespread use for nanopatterning of photoresists [26-28].

As well as requiring lower laser fluxes as they originate from lower ion stages, plasma emission based on these transitions has the advantage of being less optically thick since it is well known that the emission from Δn = 1 transitions shifts almost monotonically to higher energy with increasing ion stage so that radiation trapping amongst overlapping transitions is not a problem. In addition, the emission from satellites, which are favored in emission from solid targets, can to some extent fill in the regions between the resonance arrays in adjacent stages giving an almost continuous distribution of intensity [19].

Figure 4 shows the time-integrated spectra from C, Si_3N_4, Mo, Zr and Bi plasmas recorded at a laser intensity of 5 × 10^{11} W/cm^2 with a 10-ns pulse duration in the 2–9 nm region. For the lighter two elements, as is well known, spectra are dominated by H and He like ion emission, while for Mo and Zr the spectra are dominated in the water window region by Δn = 1, 3*d*–4*f* transitions. Indeed, from the available literature it was possible to identify all of the strong peaks in the 2.3–4.2 nm region of the Mo spectrum and assign them to ion stages from Mo^{14+} to Mo^{21+}. From Fig. 4 it is obvious that the main contribution from Mo plasmas to the water window region begins at a wavelength lower than 3.5 nm. In order to have greater wavelength coverage, a lower Z target where the corresponding isoelectronic emission is displaced to longer wavelength is a more suitable choice. This consideration allied to the fact that each in these spectra emission from adjacent ion stages is displaced by 0.3–0.5 nm in successive ion stages suggested that Zr plasmas should provide the optimum water widow coverage.

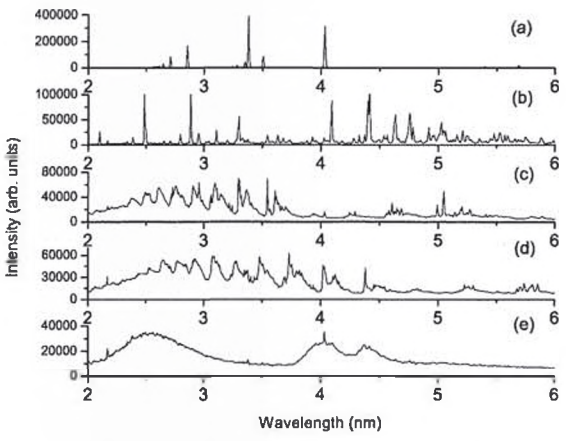

Fig. 4. Spectral behaviors of the Bi plasmas in the laser intensity dependence on the observed emission spectra (a), the peak wavelength of the n = 4–4 transition (circles) and the n = 4–5 transition (rectangles) (b).

The spectrum of Bi is also shown in this figure for comparison and while the $n = 4–n = 4$ UTA emission is quite intense near 4 nm and the $4f–5g$ transitions contribute to a broad Gaussian shaped feature centered near 2.5 nm, the overall emission does not "fill" the water window region as completely as that from Zr targets.

In Fig. 5 we present the variation of spectral emission for a range of power densities. While the intensity increases with the laser intensity, the appearance of the spectrum changes only slightly, with short wavelength features being more distinct higher than 10^{13} W/cm^2. The corresponding electron temperatures are evaluated to range from 100–200 eV while calculations within the collisional-radiative (CR) framework indicate that plasmas with peak temperatures of at least 230 eV are required to optimize the water window emission [17].

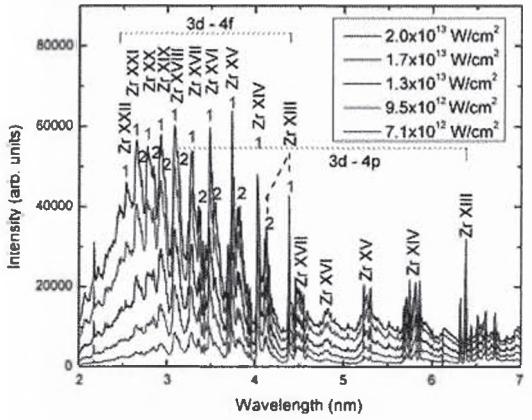

Fig. 5. Spectral behavior of Zr plasmas showing the laser intensity dependence of the observed emission spectra. Resonant $3d–4f$ (1) and $3d–4p$ transitions as well as satellite lines from $3d^{n-1}4s4f–3d^{n-2}4s4f$ (2) are clearly seen for $Zr^{12+}–Zr^{21+}$ in this figure.

In order to make a relative comparison of the total emission, the total number of counts was integrated between 2.3 and 4.2 nm for each of the targets shown in Fig. 4 for the range of power densities covered in the experiments. The results are shown for both ns and ps pulse irradiation in Fig. 6 and show that the total emission in the 10 ns plasmas is some 50% greater in the case of Mo and Zr while it is almost 50% less in the case of Bi. This results from the need to have significantly higher ion stages and therefore a hotter plasma for efficient Bi emission which is favored at the higher laser flux. In order to obtain $4f–5g$ emission the ion stages must lie in the range from Bi^{22+} to Bi^{35+}, while for strong $4p–4d$ and $4d–4f$ transitions ions must possess an open $4d$ subshell ($Bi^{36+}–Bi^{45+}$). It is interesting also to compare the total flux available from C and N containing plasmas; while the intensity of the individual lines is certainly greater, the total in-band emission is significantly less than for any of the higher Z targets. In addition, it is interesting to note that while the C emission is consistently stronger than that from the Si_3N_4 in the ps laser-produced plasmas, for ns plasmas the behavior is more complex and the emission of Si_3N_4 exceeds that of C plasmas at both lowest and highest laser fluxes used for 10-ns irradiation.

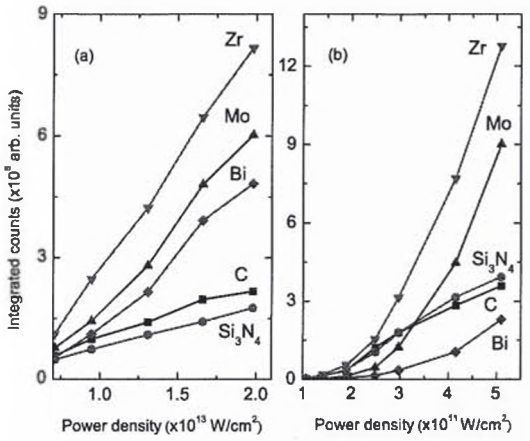

Fig. 6. Water window emission (total counts) as a function of power density for 150 ps (a) and 10 ns (b) laser pulses showing the variation of total count rate for plasmas of the elements presented in Fig. 4.

Since the intensity depends on both photon energy and count rate, in order to get a measure of the total flux, the quantity $N(E)EdE$, where $N(E)$ is the number of counts occurring at energy E, was integrated over the water window and the results yielded curves very similar to those of Fig. 6 and again showed that of the elements considered here, Zr

is the brightest emitter in the water window for laser fluxes in the 10^{12}–10^{13} W/cm^2 range.

6. Summary

We have demonstrated high-efficiency emission in the water window spectral region based on laser-produced Zr and Bi plasmas, and have proposed methods to increase it still further. Resonance emission from multiply charged ions merges to produce intense UTA, extending to wavelengths below the carbon K edge. The overall spectral behavior is well described by simulations. The experimental results also provide an outline for the design concept for single-shot cell imaging with a novel microscope optical system. The method presented here opens the way for applications in next-generation biological science.

Acknowledgements

The authors are deeply indebted to Prof. Weihua Jiang (Nagaoka University of Technology), Prof. Akira Endo (HiLASE Project, Institute of Physics AS), for useful discussion. The authors are grateful to Takamitsu Otsuka, Bowen Li, Yusuke Suzuki, and Ryoichi Hirose for their unparalleled technical support. A part of this work was performed under the auspices of MEXT (Ministry of Education, Culture, Science and Technology, Japan) and was also supported by the high education donation program funded by Intel K.K., which is a subsidiary of Intel Corp. One of the authors (T.H) also acknowledges support from The Canon Foundation and Research Grant (Basic Research) on TEPCO Memorial Foundation. The UCD group is supported by Science Foundation Ireland under Principal Investigator Research Grant No. 07/IN.1/I1771. We are also grateful to Gigaphoton Inc. for providing the picosecond laser system.

References

[1] J. C. Solem and G. C. Baldwin, *Science,* **218**, 229 (1982).

[2] T. Gorniak et al., *Opt. Exp.* **19**, 11059 (2011).

[3] P. A. C. Jansson et al., *Rev. Sci. Instrum.*, **76**, 043503 (2005).

[4] P. A. C. Takman et al., *J. Microsc.*, **226**, 175 (2007).

[5] P. Skoglund et al., *Appl. Phys. Lett.*, **96**, 084103 (2010).

[6] "EUV Sources for Lithography", edited by V. Bakshi (SPIE, Bellingham, WA, 2005).

[7] T. Otsuka et al., *Appl. Phys. Lett.*, **97**, 111503 (2010).

[8] T. Otsuka et al., *Appl. Phys. Lett.*, **97**, 231503 (2010).

[9] T. Higashiguchi et al., *Appl. Phys. Lett.*, **99**, 191502 (2011).

[10] C. Wagner and N. Harned, *Nat. Photonics*, **4**, 24 (2010).

[11] D. Kilbane, *J. Phys. B: At. Mol. Opt. Phys.*, **44**, 165006 (2011).

[12] B. Li et al., *Proc. SPIE*, **8139**, 81390P (2011).

[13] T. Higashiguchi et al., *SPIE Newsroom* (DOI: 10.1117/2.1201109.003765, 2011).

[14] P. K. Carroll and G. O'Sullivan, *Phys. Rev. A*, **25**, 275 (1982).

[15] G.-M. Zeng et al., *J. Appl. Phys.*, **67**, 3597 (1990).

[16] G.-M. Zeng et al., *J. Appl. Phys.*, **69**, 7460 (1991).

[17] D. Colombant and G. F. Tonon, *J. Appl. Phys.*, **44**, 3524 (1973).

[18] T. Higashiguchi et al., *Appl. Phys. Lett.*, **100**, 014103 (2012).

[19] B. Li et al., *Appl. Phys. Lett.*, **102**, 041117 (2013).

[20] K. Sakano and M. Yamamoto, *Proc. SPIE*, **3767**, 238 (1999).

[21] R. D. Cowan, "The Theory of Atomic Structure and Spectra" (University of California Press, Berkeley, 1981).

[22] M. Bertilson et al., *Opt. Exp.*, **17**, 11057 (2009).

[23] H. Tanaka et al., *Appl. Phys. Lett.*, **87**, 041503 (2005).

[24] Y. Ueno et al., *Appl. Phys. Lett.*, **90**, 191503 (2007).

[25] S. P. Kruger et al., *Opt. Exp.*, **18**, 13492 (2010).

[26] T. Gowa et al., *J. Photopolym. Sci. Technol.*, **22**, 273 (2009).
[27] T. Gowa et al., *Radiat. Phys. Chem.*, **80**, 248 (2011).
[28] T. G. Oyama et al., *AIP Advances*, **1**, 042153 (2011).